Wavelet Based Multifractal Analysis of Rough Surfaces: Application to Cloud Models and Satellite Data

J. Arrault* and A. Arnéodo
Centre de Recherche Paul Pascal, Avenue Schweitzer, 33600 Pessac, France

A. Davis and A. Marshak
Climate & Radiation Branch, NASA's Goddard Space Flight Center, Greenbelt, Maryland 20771
(Received 6 March 1997)

The wavelet transform modulus maxima (WTMM) method is generalized to multifractal image analysis, providing a statistical characterization of the fluctuating roughness of fractal surfaces. This isotropic 2D version of WTMM methodology is calibrated on deterministic self-similar interfaces and random self-affine surfaces (fractional Brownian surfaces and multifractal counterparts). Applications to high-resolution satellite data and simulated radiance fields for stratocumulus clouds are presented. [S0031-9007(97)03555-2]

PACS numbers: 47.53.+n, 02.50.Fz, 05.40.+j, 92.60.Nv

Since the late 1970's, there have been numerous applications of fractal ideas [1] to surface science. Indeed, a wide variety of natural and technological processes generate complex interfaces [2]. Numerical techniques have been designed for interfaces that are isotropic and self-similar when magnified equally in all directions and provide good estimates of the fractal dimension D_F [1,2]. However, in the presence of anisotropic scale invariance, different methods of computing D_F yield different results [3]. Alternatively, one can compute the so-called roughness exponent H (supposedly equal to the codimension $d - D_F$) describing the dependence of the interface's width with measurement scale [1,2]. Unfortunately D_F and H are global quantities that do not account for the possibility of point-to-point fluctuations in the local regularity of a fractal surface. Box-counting and correlation algorithms were successfully adapted [2] to resolve multifractal scaling for isotropic self-similar fractals by computation of the generalized fractal dimensions D_q. As to self-affine fractals, Frisch and Parisi [4] proposed, in the context of turbulence analysis, an alternative multifractal description based on the scaling behavior of structure functions: $S_p(l) = \langle(\delta f_l)^p\rangle \sim l^{\zeta_p}$ (p integer > 0), where $\delta f_l(x) = f(x + l) - f(x)$ is an increment of the recorded signal f over distance l. Then, after reinterpreting the roughness exponent as a local quantity [$|\delta f_l(x)| \sim l^{h(x)}$], the $D(h)$ singularity spectrum is defined as the Hausdorff dimension of the set of points x where the local roughness (or Hölder) exponent $h(x)$ of f is h. In principle $D(h)$ can be attained by Legendre transforming the ζ_p's. There are, however, some fundamental drawbacks to the structure function method [5]. Indeed, it generally fails to fully characterize $D(h)$ since only the strongest singularities of f are *a priori* amenable to this analysis [$S_p(l)$ does not exist for $p < 0$]. Moreover, singularities corresponding to $h > 1$, as well as regular behavior, bias the estimate of ζ_p. A new approach to multifractal analysis based on the continuous wavelet transform (WT) [5] uses the scaling of partition functions computed from the wavelet transform modulus maxima (WTMM). The WTMM method allows a complete statistical analysis of the roughness fluctuations of a self-affine function through the entire $D(h)$ singularity spectrum. Applications of this method to 1D signals have provided insight into a wide variety of outstanding problems, notably in fully developed turbulence [5,6], fractal growth phenomena [7], and "DNA walk" statistical analysis [8]. In this Letter we generalize the WTMM method from 1D to 2D, with the specific goal to analyze the multifractal properties of rough surfaces with fractal dimension D_F between 2 and 3.

There is an increasing interest in the application of the WT to image processing [9,10]. Mallat *et al.* [9] have extended the WTMM representation in 2D in a manner inspired from Canny's multiscale edge detectors. The idea is to first smooth the digital image by convolution with a filter, then compute the gradient of the smooth signal. Define two wavelets: $\Psi_1(x, y) = \partial\theta(x, y)/\partial x$ and $\Psi_2(x, y) = \partial\theta(x, y)/\partial y$, where $\theta(x, y)$ is a 2D smoothing function well localized around $x = y = 0$. For any function $f(x, y) \in L^2(\mathbf{R}^2)$, the WT defined with respect to Ψ_1 and Ψ_2 can be expressed as a vector [9]:

$$\boldsymbol{T}_\Psi[f](\boldsymbol{b}, a) = \boldsymbol{\nabla}\{T_\theta[f](\boldsymbol{b}, a)\}, \tag{1}$$

where $T_\theta[f](\boldsymbol{b}, a) = a^{-2}\int\int_{-\infty}^{+\infty}\theta(\frac{\boldsymbol{r}-\boldsymbol{b}}{a})f(\boldsymbol{r})\,d^2\boldsymbol{r}$. If θ is an isotropic wavelet, then $T_\theta[f](\boldsymbol{b}, a)$ is a continuous 2D WT of f as originally defined by Murenzi [11]. If instead θ is just a smoothing filter such as a Gaussian, $\theta(\boldsymbol{r}) = \exp(-\boldsymbol{r}^2/2)$, then Eq. (1) defines the 2D WT as the gradient vector of $f(\boldsymbol{r})$ smoothed by dilated versions $\theta(\boldsymbol{r}/a)$ of this filter. Mallat *et al.* [9] define the WTMM, at a given scale a, by finding positions $\boldsymbol{b}$ where the modulus of $\boldsymbol{T}_\Psi[f](\boldsymbol{b}, a)$ is locally maximum in the direction of the gradient vector $\boldsymbol{T}_\Psi[f]$. The so-defined WTMM leads to an efficient analysis of the local regularity of f via the

Hölder exponent $h(\boldsymbol{r})$ $(0 \leq h \leq 1)$. However, we do not know *a priori* whether f itself or one of its derivatives is singular at any given point. We therefore extend the Hölder exponent concept to that of singularity strength as defined by the largest exponent such that there exists a polynomial P_n of order n satisfying $|f(\boldsymbol{r}) - P_n(\boldsymbol{r} - \boldsymbol{r}_0)| \leq C|\boldsymbol{r} - \boldsymbol{r}_0|^{h(\boldsymbol{r}_0)}$, for $\boldsymbol{r}$ in the neighborhood of $\boldsymbol{r}_0 = (x_0, y_0)$. If $n < h(\boldsymbol{r}_0) < n + 1$, then f is n (but not $n + 1$) times differentiable at $\boldsymbol{r}_0$. Thus the higher the exponent $h(\boldsymbol{r}_0)$, the more regular the function f around $\boldsymbol{r}_0$. It is now straightforward to generalize the Mallat *et al.* result [9]. Provided the first n moments of the wavelet $\boldsymbol{\Psi}$ vanish (e.g., $\boldsymbol{\Psi}$ is the nth derivative of the Gaussian), the WTMM behaves like [12]

$$|\boldsymbol{T}_\Psi[f](\boldsymbol{r}_0, a)| = \{T^2_{\Psi_1}[f](\boldsymbol{r}_0, a) + T^2_{\Psi_2}[f](\boldsymbol{r}_0, a)\}^{1/2} \sim a^{h(\boldsymbol{r}_0)}, \tag{2}$$

as we follow the WT "skeleton" defined by the WTMM, from large to small scales down to the point $\boldsymbol{r}_0$. Because of its "scanning" and "zooming" capabilities, the 2D WT is a mathematical microscope that sees the fluctuations of roughness in self-affine surfaces [via local estimatation of the Hölder exponent $h(\boldsymbol{r})$]. Equation (2) allows us to follow the strategy elaborated for multifractal analysis of 1D signals [5]. The 2D WTMM method thus consists in defining partition functions with wavelet coefficients from the WTMM skeleton [12]:

$$\mathcal{Z}(q, a) = \frac{1}{a} \sum_{l \in \mathcal{L}(a)} \int |\boldsymbol{T}_\Psi[f][s_l(a), a]|^q \, ds_l \sim a^{\tau(q)}, \tag{3}$$

where $\mathcal{L}(a)$ is the set of all maxima chains at scale a and $s_l(a)$ is the curvilinear coordinate along the chain l. Note that the exponent $\tau(q)$, $q \in \mathbf{R}$, has well-known meaning for some specific values of q: (i) $-\tau(0)$ is the fractal dimension of the set of singularities of f, (ii) $\tau(1)$ is related to the capacity dimension $D_C(\mathcal{G}) = \max[2, 2 - \tau(1)]$ of the graph $\mathcal{G}$ of f, generally equal to D_F, and (iii) $\tau(2)$ is related to the scaling exponent β of the spectral density $S(\boldsymbol{k}) = |\hat{f}(\boldsymbol{k})|^2 \sim |\boldsymbol{k}|^{-\beta}$ with $\beta = 4 + \tau(2)$. A statistical characterization of the fluctuations of regularity of a self-affine function $f(x, y)$ can then be achieved by determining the $D(h)$ singularity spectrum from the Legendre transform of $\tau(q)$ [512]: $D(h) = \min_q[qh - \tau(q)]$.

Figure 1 illustrates how the 2D WTMM enlighten the hierarchical distribution of singularities in a tutorial example, a (zero-area) "snowflake" fractal. We first focus our WT microscope on the one-scale snowflake fractal shown in Fig. 1(a). The WTMM chains computed at scales $a = 1/3$ and $1/3^2$ are also shown in Fig. 1(a). Figure 1(b) shows the WTMM skeleton obtained by continuously joining these chains over a finite range of scales. The branching structure of this skeleton clearly reveals the construction rule of the one-scale snowflake fractal [11].

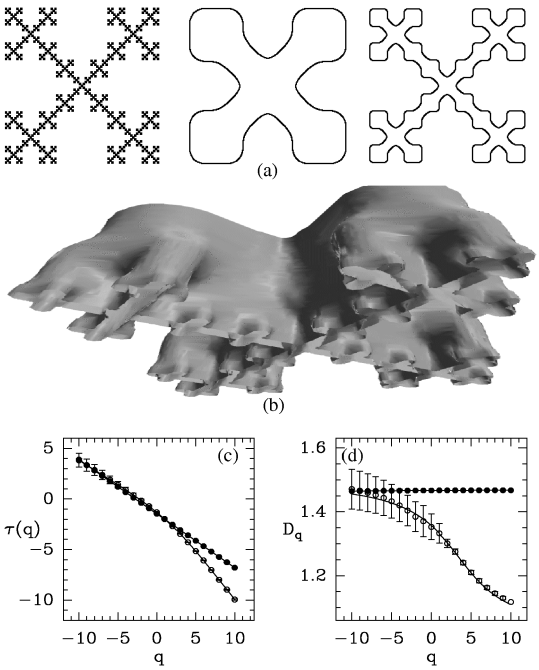

FIG. 1. 2D WTMM analysis of self-similar snowflake fractals. $\theta(x, y)$ is the Gaussian function. (a) The one-scale snowflake and associated WTMM chains at scale $a = 1/3$ and $1/3^2$. (b) Perspective view of the WTMM skeleton. (c) $\tau(q)$ vs q. (d) D_q vs q. In (c) and (d): (•) homogeneous one-scale snowflake and (∘) multifractal two-scale snowflake.

As $a \to 0$, the WTMM chain provides a better and better approximation of the snowflake interface. Figure 1(c) shows results obtained with the 2D WTMM method for the partition function scaling exponents $\tau(q)$. According to Eq. (3), those exponents were computed from linear regressions of $\ln \mathcal{Z}(q, a)$ versus $\ln a$ over about two decades in scale, corresponding to four steps of the construction process. This $\tau(q)$ is linear in q, as expected for homogeneous fractals. Figure 1(d) shows that our numerical results for $D_q = [\tau(q) + 2q]/(q - 1)$ agree with theory [11]: $D_q = \ln 5/\ln 3$, independently of q. Figures 1(c) and 1(d) also show results of similar analyses of a two-scale snowflake fractal [11]; $\tau(q)$ is now a concave nonlinear function which translates to decreasing D_q's, the hallmark of multifractal scaling. The agreement between our numerics and theory demonstrates that our WTMM method can quantify geometrical multifractality in 2D.

Fractional Brownian functions $B_H(x, y)$ are Gaussian stochastic processes with stationary increments, often used to generate random self-affine surfaces [1–3] with known statistical properties: $\tau(q) = qH - 2$, $0 < H < 1$. We tested the 2D WTMM technique on ten 512×512 realizations of B_H for various values of H ($1/2$ corresponds to uncorrelated increments, increments being correlated for any other value). We focus here on the uncorrelated case $B_{1/2}$ since it has a k^{-3} power spectrum, similar to that of the radiance field investigated further on. Figure 2(a) shows a realization of $B_{1/2}$ and Fig. 3(a)

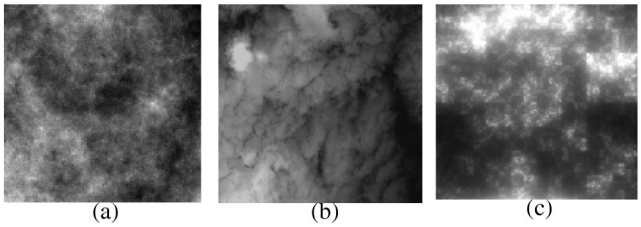

FIG. 2. 256 grey-scale coding of 512×512 images. (a) Brownian surface $B_{H=1/2}$. (b) Portion of a LANDSAT image of typical marine stratocumulus off the coast of Southern California. (c) Synthetic radiance field computed with a fractionally integrated singular cascade model.

the scaling of $\log_2[a^2 \mathcal{Z}(q,a)]/q$ versus $\log_2 a$ for different values of q; over a large range of scales, the data fall on straight lines that are quite parallel. Figure 3(c) displays $\tau(q)$ as estimated by linear regression from Eq. (3). Statistical convergence is achieved for $-2 < q < 6$ and the data fall on a line of slope $h = \partial\tau/\partial q = H = 1/2$. From linear regressions in Fig. 3(a), we confirm that the slopes $[\tau(q) + 2]/q$ are equal to $H = 1/2$, within numerical uncertainty. We obtained equally satisfactory results when investigating B_H for other values of H. As expected from the Legendre transform of $\tau(q)$, these model surfaces are nowhere differentiable with a unique Hölder exponent [1,3]: $h = H$ and $D(h = H) = 2$. Further evidence for this roughness homogeneity appears in Fig. 4(a) showing the WT probability distribution function (pdf) $P(T_\theta(.,a))$, at different scales a. When increasing a, the pdf's become wider and wider but, by plotting $\ln P$ versus T_θ/a^H, they all collapse onto a single curve which is well approximated by a parabola, as expected for Gaussian processes.

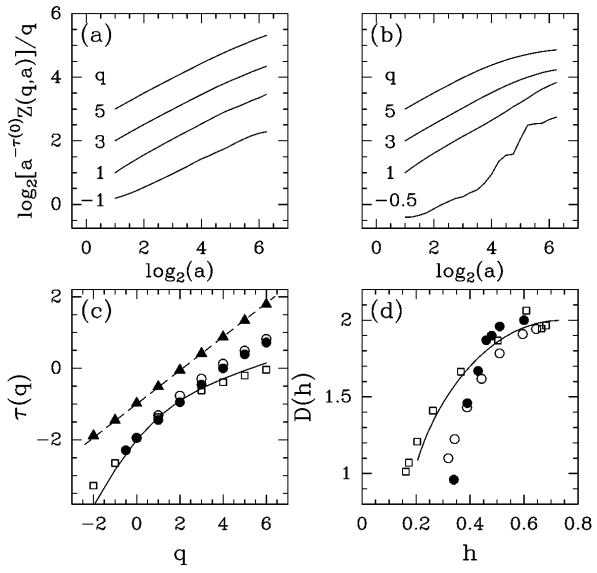

FIG. 3. WTMM estimates of $\tau(q)$ and $D(h)$ for rough surfaces. $\theta(x,y)$ is the Gaussian function. $\log_2[a^2 \mathcal{Z}(q,a)]/q$ vs $\log_2 a$, for different q, from a sample of (a) ten Brownian surfaces $B_{H=1/2}$ and (b) 32 LANDSAT subscenes. (c) $\tau(q)$ vs q. (d) $D(h)$ vs h. In (c) and (d): (▲) $B_{H=1/2}$, dashed line in (c) is the theoretical $\tau(q) = q/2 - 2$ (for clarity the data have been shifted upward by $+1$); (•) LANDSAT radiance data; (□) fractionally integrated cascade model; the continuous lines correspond to the theoretical spectra; (∘) synthetic radiance field.

Fractal analysis of atmospheric data has gained considerable momentum since Lovejoy's seminal paper [13] on the area-perimeter relation for clouds and rain. Multifractal approaches have since been imported into meteorology from statistical fluid dynamics and deterministic chaos. Cloud structure has been probed internally by radiosondes and aircraft and remotely observed with high-resolution satellite imagery. *In situ* cloud data reveal strong variability of many quantities of interest; for instance, 1D transects of liquid water density obey multifractal statistics over at least three decades in scale [14]. Satellite imagery has been processed only by spectral or box-counting methods [2]. Being at once persistent and horizontally extended, marine stratocumulus (Sc) layers are responsible for a large portion of the Earth's global albedo, hence its overall energy balance (i.e., climate). This motivates us to apply 2D WTMM methodology to characterize marine Sc structure. We start with a large ($\simeq$120 km^2 $\times$ 120 km^2) completely cloudy LANDSAT scene [15] captured with the Thematic Mapper camera ($\simeq$30 m resolution) in the 0.6–0.7 μm channel. Figure 2(b) shows a typical 512×512 portion of the original (4096×4096) image where quasi-nadir viewing radiance at satellite level is digitized on an eight-bit grey scale. To minimize spurious saturation effects, WTMM analysis was applied only to one half of the data that is only 7% saturated, namely, 32 selected 512×512 subscenes. Figure 5 shows maxima chains computed with Eq. (1), taking θ as Gaussian, at three different scales. The $\tau(q)$ curve in Fig. (c), extracted from the scaling behavior of the partition functions defined on these maxima chains [Eq. (3)], deviates from a straight line in contrast with homogeneous Brownian surfaces. We note the agreement between $\tau(2) = -0.91 \pm 0.03$ and the estimated spectral exponent $\beta = 3.00 \pm 0.05 \simeq \tau(2) + 4$. Figure 3(b) shows $\log_2[a^2 \mathcal{Z}(q,a)]/q$ versus $\log_2 a$ for

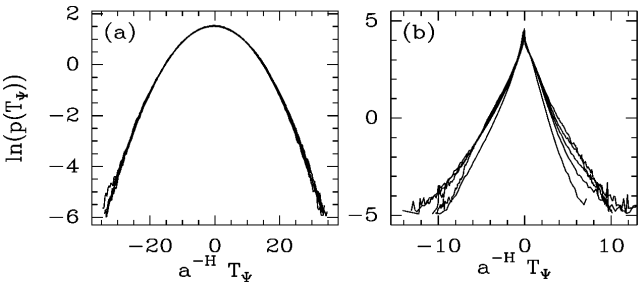

FIG. 4. Pdf's of rescaled WT coefficients. Murenzi's 2D continuous WT [11] is used at scales $a = a_0$, $a_0/2$, $a_0/4$, $a_0/8$. The analyzing wavelet θ is the Mexican hat. $\ln P$ vs $T_\theta a^{-H}$ for (a) ten Brownian surfaces $B_{1/2}$ with $H = 1/2$ and (b) 32 LANDSAT subimages with $H = 0.6 = h(q = 0)$, i.e., the most frequent Hölder exponent.

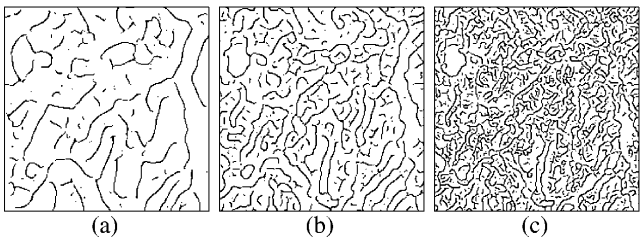

FIG. 5. WTMM maxima chains of the LANDSAT subimage in Fig. 2(b) at different scales: (a) $a = a_0$, (b) $a = a_0/2$, and (c) $a = a_0/4$. $\theta(x, y)$ is the Gaussian function.

a number of q's; apart from finite-size effects at large scales, scaling is recovered over about a decade ([400 m, 4000 m]) for $q > 0$ and the slopes $[\tau(q) + 2]/q$ depend on q, thus confirming the nonlinearity of $\tau(q)$. For $q < 0$, the scaling unfortunately deteriorates, probably due to sampling and saturation effects. Figure 3(d) shows the $D(h)$ singularity spectrum. More precisely, we obtain its increasing left part ($q = \partial D/\partial h > 0$), from which one can say that the strongest singularities have $h_{\min} = 0.33 \pm 0.03$, while the most frequent ones have $h(q = 0) = 0.60 \pm 0.02$. The maximum value $D(h(q = 0)) = -\tau(0) = 2.00 \pm 0.03$ implies that the radiance field is everywhere singular. Figure 4(b) shows the same computation of the pdf $P(T_\theta(., a))$ at different scales as in Fig. 4(a) for Brownian surfaces. We find (i) that no single value of H collapses all the pdf's onto a unique distribution, an additional test of the multifractality of marine Sc and (ii) that the pdf's tails are similar to the stretched exponential behavior observed for the statistics of velocity increments in fully developed turbulence [16].

Schertzer and Lovejoy [17] proposed fractionally integrated (i.e., power-law filtered) singular cascades as scale-invariant models for clouds. Upon fractional integration in $d = 2$ space of the measures obtained by the "p model" [14,18], one generates self-affine functions with $h(\mathbf{r})$ fluctuating from point to point. In Fig. 3(c), the 2D WTMM estimates of $\tau(q)$ (based on ten 512×512 synthetic images) are compared to theory [14] $\tau(q) = -(q + 1) - \log_2[p^q + (1 - p)^q] + qH^*$, where $p(> 1/2)$ and $1 - p(< 1/2)$ are the multiplicative weights and H^* is the exponent of the power-law filter. Good agreement is found for $-1 \leq q \leq 5$ for this limited sample, a test of the reliability of our methodology to resolve multifractal scaling of rough surfaces. Finally, the "independent pixel" approximation can be invoked to compute the radiance field for the cloud model at the scales of interest here [15] [Fig. 2(c)]. Using the 2D WTMM method, we found values for the structural and optical parameters for the cloud model ($p = 0.32$ and $H^* = 0.64$) that give very close $\tau(q)$ [Fig. 3(c)] and $D(h)$ [Fig. 3(d)] spectra for the artificial radiance fields and the LANDSAT data.

We thank E. Bacry, R. Cahalan, N. Decoster, J. F. Muzy, F. Tallet, and W. Wiscombe for stimulating discussions and technical assistance. This work was supported by NATO (Grant No. CRG 960176), and by U.S. Department of Energy (Grant No. DE-A105-90ER61069). Dr. Cahalan (NASA/GSFC) is acknowledged for the LANDSAT data from the FIRE archive.

*Present address: The University of Edinburgh, Mayfield Road, Edinburgh, EH9 3JZ, United Kingdom.

[1] B. B. Mandelbrot, *The Fractal Geometry of Nature* (Freeman, San Fransisco, 1982).
[2] J. Feder, *Fractals* (Pergamon, New York, 1988); *Dymanics of Fractal Surfaces,* edited by F. Family and T. Vicsek (World Scientific, Singapore, 1991); *Fractals in Geoscience and Remote Sensing,* edited by G. Wilkinson *et al.,* Image Understanding Research Series Vol. 1 (ECSC-EC-EAEC, Brussels, Luxembourg, 1995).
[3] *The Science of Fractal Images,* edited by H. O. Peitgen and D. Saupe (Springer, New York, 1987); B. Dubuc *et al.,* Phys. Rev. A **39**, 1500 (1989); B. Lea Cox and J. S. Y. Wang, Fractals **1**, 87 (1993).
[4] U. Frisch and G. Parisi, in *Turbulence and Predictability in Geophysical Fluid Dynamics and Climate Dynamics,* edited by M. Ghil *et al.* (North-Holland, Amsterdam, 1985), p. 84.
[5] J. F. Muzy, E. Bacry, and A. Arnéodo, Phys. Rev. Lett. **67**, 3515 (1991); Phys. Rev. E **47**, 875 (1993); Int. J. Bifurcation Chaos **4**, 245 (1994).
[6] A. Arnéodo, J. F. Muzy, and S. G. Roux, J. Phys. II (France) **7**, 363 (1997).
[7] A. Arnéodo *et al.,* Phys. Rev. Lett. **68**, 3456 (1992).
[8] A. Arnéodo *et al.,* Physica (Amsterdam) **96D**, 291 (1996).
[9] S. Mallat and W. L. Hwang, IEEE Trans. Inform. Theory **38**, 617 (1992); S. Mallat and S. Zhong, IEEE Trans. Patt. Anal. Mach. Intell. **14**, 710 (1992).
[10] J. P. Antoine *et al.,* Signal Processing **31**, 241 (1993).
[11] R. Murenzi, Ph.D. thesis, University of Louvain la Neuve, 1990; F. Argoul *et al.,* Phys. Rev. A **41**, 5537 (1990).
[12] J. Arrault, Ph.D. thesis, University of Bordeaux 1, 1995.
[13] S. Lovejoy, Science **216**, 185 (1982).
[14] A. Davis *et al.,* J. Geophys. Res. **99**, 8055 (1994); A. Marshak *et al.,* J. Atmos. Sci. **54**, 1423 (1997).
[15] A. Davis *et al.,* J. Atmos. Sci. **54**, 241 (1996).
[16] Y. Gagne, Ph.D. thesis, University of Grenoble, 1987; P. Kailasnath *et al.,* Phys. Rev. Lett. **68**, 2766 (1992); P. Tabeling *et al.,* Phys. Rev. E **53**, 1613 (1996).
[17] D. Schertzer and S. Lovejoy, J. Geophys. Res. **92**, 9693 (1987).
[18] C. Meneveau and K. R. Sreenivasan, Phys. Rev. Lett. **59**, 1424 (1987).